Three-Dimensional Dynamic Rupture Simulations on Partially-Creeping Strike-Slip Faults

Julian C. Lozos[1], David D. Oglesby[2], and Gareth J. Funning[2]

[1]California State University, Northridge
[2]University of California, Riverside

Corresponding Author: Julian C. Lozos (julian.lozos@csun.edu)

Key Points:

- Patches of aseismic creep can be barriers to rupture, depending on their positions and dimensions.
- Rupture can propagate around creeping zones only if there is a wide enough locked area to maintain directivity and rupture energy.
- Rate-strengthening friction in creeping zones depletes the energy of the rupture front until it stops.

Abstract

Partially creeping faults exhibit complex behavior in terms of which parts of the fault slip seismically versus aseismically. The specific geometry of creeping versus locked fault patches may pose constraints on rupture lengths on partially-creeping faults. We use the 3D finite element method to conduct dynamic rupture simulations on simplified partially-creeping strike-slip faults, to determine whether coseismic rupture can propagate into creeping regions, and how the presence and distribution of creeping regions affects the ability of rupture to propagate across the whole fault. We implement rate-state friction, in which locked zones are represented by rate-weakening behavior and creeping zones are assigned rate-strengthening properties. We model two simplified geometries: a locked patch at the base of a creeping fault and a creeping patch at the surface of a locked fault. In the case of a locked patch within a creeping fault, rupture does not propagate far past the edges of the locked patch, regardless of its radius. The case of a creeping patch within a locked fault is more complicated. The width of the locked areas around the creeping patch determine whether rupture is able to propagate around the creeping patch. Although rupture is always able to propagate at least a small distance into the creeping patch, if the width of the locked zone between the edge of the creeping patch and the end of the fault is too narrow, rupture stops. This simplified parameter study may be useful for understanding first-order behaviors of real-world partially-creeping strike-slip faults.

1 Introduction

Partially-creeping faults are faults which sustain both non-episodic, measurable surface creep, and large-scale dynamic rupture. Partial creep defines the base and the top of the seismogenic zone in subduction zones (e.g. *Shibazaki and Shimamoto* [2007], *McCaffrey et al.* [2008]), but it also occurs on strike-slip faults around the world, most famously in the northern San Andreas Fault system in California (e.g. *Schulz et al.* [1982]; *Lienkaemper et al.* [2014]; *Murray et al.* [2014]). Variations in creep may be spatial, with patches of creep within a locked fault or vice versa, as is the case with the Hayward Fault in the San Francisco Bay Area (e.g. *Lienkaemper et al.* [1991]) or the San Andreas Fault near Parkfield (e.g. *Harris and Segall* [1987], *Waldhauser et al.* [2004]). They may also be temporal, where patches that seem to creep interseismically rupture coseismically, as in the 2011 Tohoku, Japan earthquake (e.g. *Kodaira et al.* [2012]); or faults which appeared fully locked creep following a rupture, as in the 2014 South Napa, California earthquake (e.g. *Lienkaemper et al.* [2016]; *Floyd et al.*[2016]) or following an earthquake on another fault, as with the Garlock Fault following the 2019 Ridgecrest, California earthquake (e.g. *Barnhart et al.* [2019]; *Bilham and Castillo* [2020]).

The observation that locked and creeping patches may exist on the same fault, and that the same patches of fault may creep or rupture at different points in the earthquake cycle, poses important questions for fault dynamics. There is the matter of how rupture negotiates the frictional and stress complexity that comes with a partially-creeping fault releasing stress interseismically, of how that behavior controls the endpoints of such ruptures, and of how rupture lengths and positions may or may not change over multiple seismic cycles. Here, we use dynamic rupture modeling to focus on the issue of how variation in creeping/locking properties along a strike-slip fault affects rupture behavior in a single earthquake.

Dynamic rupture models are frequently used in parameter studies on the effects of complex fault geometry and stress state on rupture behavior and termination (e.g. *Harris and Day* [1993]; *Kame et al*. [2003]; *Oglesby* [2008]; *Lozos et al*. [2011]; *Harris et al.* [2018]; *Wang et al.* [2020]). Dynamic modeling has also been used to investigate how varying individual frictional and weakening parameters affects rupture behavior (e.g. *Nielsen et al*. [2000]; *Kaneko et al.* [2008]; *Ryan and Oglesby* [2014]; *Lozos et al.* [2014]).

In the specific context of dynamic rupture on a partially-creeping strike-slip fault, we are only aware of dynamic rupture modeling studies related to specific real-world faults. *Lozos et al.* [2015] conducted models of ruptures on the partially-creeping Bartlett Springs fault in northern California, and found that reduced shear stress due to creep prevented coseismic rupture from propagating through the entire fault. *Stephenson and Lapusta* [2018] modeled ruptures across the creeping section of the San Andreas Fault in central California, and found that rupture could only propagate through if strong dynamic weakening was imposed. *Harris et al.* [2019] modeled ruptures across the Calaveras-Hayward-Rodgers Creek fault network in the San Francisco Bay Area, and found that creeping patches prevented rupture from propagating through the entire system of faults regardless of nucleation location. *Lozos and Funning* [submitted to this issue] modeled the Hayward Fault alone, and also found that frictional and stress contrasts associated with creep kept rupture confined to locked patches. The only partially-creeping fault parameter studies of which we are aware are on subduction zones (e.g. *Noda and Lapusta* [2013]), which have considerably different kinematics from strike-slip faults.

In the present study, we conduct a series of dynamic rupture models for two different simplified cases of a vertical, planar, partially-creeping strike-slip fault: one in which a patch of surface creep is embedded near the surface in a predominantly locked fault, and one in which a locked patch is embedded at the base of a predominantly creeping fault.

2 Methods

We use FaultMod [*Barall*, 2009], a 3D finite element code which has performed consistently in the Southern California Earthquake Center's dynamic rupture code verification exercise [*Harris et al.*, 2009; *Harris et al.*, 2018], to conduct dynamic rupture models of partially-creeping planar strike-slip faults embedded in a homogeneous fully elastic half space. These models represent a single coseismic rupture, and do not incorporate the physics of the process of aseismic creep; we model only the effects of creeping zones (i.e., zones of rate-strengthening friction) on coseismic rupture propagation.

Table 1. Physical and Computational Parameters

Shear stress	75 MPa
Normal stress	120 MPa
a (rate weakening)	0.008
a (rate strengthening)	0.016 (strong), 0.014 (weak), 0.012 (neutral)
b	0.012
f_0	0.6
V_0	1×10^{-6} m/s
D_c	0.02015 m
ψ_{init}	0.135524
P wave velocity	6000 m/s
S wave velocity	3464 m/s
Density	2670 kg/m^3
Element size	200 m
Nucleation radius	3000 m
Nucleation shear stress	100 MPa

We implement rate-state friction, specifically a modified Dieterich-Ruina aging law [*Dieterich*, 1978; *Ruina*, 1983]: $\tau = a\sigma_d \text{arcsinh}[(V/2V_0)\exp((f_0+\psi)/a)]$, where state variable ψ is defined as $d\psi/dt = -(bV_0/L)(\exp(-\psi_{ss}/b)-\exp(-\psi/b))$, ψ_{ss} is the state variable at steady state, *V* is the slip rate, V_0 is a reference velocity, f_0 is a reference friction coefficient, τ is shear stress, σ_d is time-dependent normal stress, and *a* and *b* are dimensionless direct effect parameters. It is the difference between *a* and *b* that controls the overall frictional behavior of the fault. If *b-a* is positive, the steady-state friction on the fault weakens as the slip rate increases, allowing for normal dynamic rupture, while a negative *b-a* means that the fault strengthens with increased slip rate, thus promoting aseismic creep and disfavoring coseismic rupture. If *b-a* is zero, the fault is rate-neutral, meaning that it neither actively weakens with increasing slip rate, nor actively resists slip.

Laboratory friction experiments on rocks collected from creeping fault zones (e.g. *Moore and Rymer* [2007]; *Moore et al.* [2018]) show that these rocks exhibit rate-strengthening behavior. As such, there are a number of modeling studies on aseismic slip processes such as afterslip and creep events which implement rate-strengthening friction on creeping faults (e.g. *Barbot et al.* [2009], *Kaneko et al.* [2013], *Wei et al.* [2015]). We therefore follow this example and parameterize the creeping sections of our model faults with rate-strengthening friction, while the locked sections of the fault have rate-weakening properties. We use three different creep parameterizations: one with stronger rate-strengthening properties, which should be more resistant to coseismic rupture; one with weaker rate-strengthening; and one case with rate-neutral properties. In all of our models, we force nucleation within the rate-weakening zones by raising the shear stress above the yield stress and forcing rupture to propagate over a fixed radius that is larger than the critical patch size needed for self-sustaining rupture propagation. We use the same parameters as in the friction law comparison parameter study of *Ryan and Oglesby* [2014]. We list our physical and computational parameters in Table 1.

We show the geometry for our models of a creeping patch embedded within a locked fault in Figure 1. We place a semi-circular rate-strengthening patch at the top center of the fault, as a representation of a fault with measurable surface creep, similar to the Green Valley Fault and one interpretation of the Bartlett Springs Fault [*Lienkaemper et al*., 2014]. In the primary set of models, we test creeping patch radii of 4, 6, 8, 10, and 12 km, while keeping the other fault dimensions fixed, and keeping the nucleation at 3 km from the left edge of the fault and 8 km from the base of the fault. In order to test for horizontal directivity effects, we also conducted a set of models in which we extended the length of the fault as we increased the radius of the creeping patch, thus keeping the nucleation point at the same distance from the edge of the creeping patch in all cases. Similarly, we tested for vertical directivity effects by conducting a set of models in which we increased the depth of the fault as we increased the radius of the creeping patch, and varied the nucleation point such that the distance between it and the edge of the creeping patch was the same in all cases.

Figure 1.

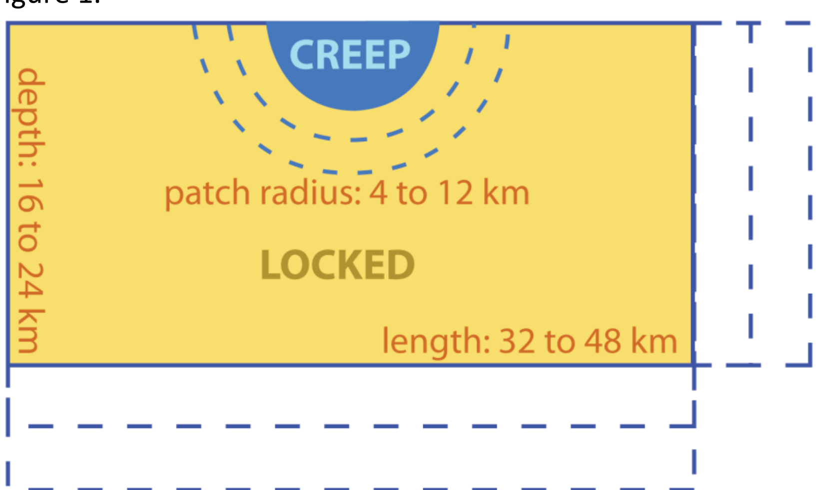

Figure 1. Cartoon of fault geometry, for models with a rate-strengthening patch embedded within an otherwise rate-weakening fault. Dotted lines indicate dimensions that we varied within our exploration of parameter space.

Figure 2 shows the geometry of our models of a locked patch embedded within a creeping fault. In these models, we place a semi-circular rate-weakening patch at the base of the fault, also to represent a fault with measurable surface creep, similar to the Hayward Fault [*Schmidt et al.*, 2005; *Funning et al.*, 2009] and another interpretation of the Bartlett Springs Fault [*Murray et al.*, 2014]. As in the previous set of models, we tested locked patch radii of 4, 6, 8, 10, and 12 km, while keeping the other fault dimensions constant. Our forced nucleation in these models is at the center of the locked patch. Because rupture directivity in these cases is controlled by the size of the locked patch, we did not conduct models with variable fault length or basal depth in this creep/locking configuration.

Figure 2.

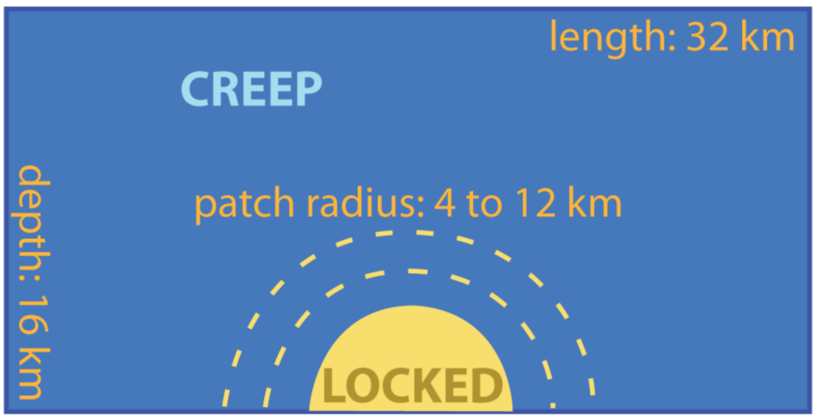

Figure 2. Cartoon of fault geometry, for models of a rate-weakening patch in an otherwise rate-strengthening fault. The radius of the locked patch is the only variable dimension here; the fault length and depth are fixed.

3 Results

3.1 Creeping Patch Within a Locked Fault

In the set of models in which we keep the fault dimensions constant but vary the radius of the creeping patch, we find that the radius of the creeping patch controls both the ability of dynamic rupture to propagate across the entire length of the fault, and the ability of the creeping patch to sustain coseismic slip. Figure 3 shows the maximum horizontal slip rate sustained across the fault in these models, using the stronger rate-strengthening properties for the creeping patches. We do not show vertical slip rate because we set these models up to produce strike-slip motion, and any dip-slip movement is negligibly small compared to the horizontal motion. We find that, if the radius of the creeping patch is half, or less than half of the seismogenic thickness of the fault, rupture is able to propagate past the creeping patch, along the full strike of the fault. In these cases, the primary rupture through the locked part of the fault progresses along strike and wraps around the creeping patch, after which point slower slip propagates inward into the creeping patch. For radii of 4 and 6 km, the entire creeping patch sustains some coseismic slip, but slip does not reach the center of the patch in the models with an 8 km or greater patch radius. In models with a patch radius of greater than half the seismogenic thickness of the fault (10 and 12 km), rupture stops within the narrow locked zone between the edge of the creeping patch and the base of the fault. In these models, the left edge of the creeping patch, closer to the forced nucleation point, sustains some slow coseismic slip, but this does not progress as far into the creeping patch as in the models where dynamic rupture is able to wrap around the patch and then propagate inward.

Using weaker rate-strengthening properties for the creeping patches does not have a first order effect on rupture's ability to propagate across the entire fault (see supplemental figures S1), though it does allow for the creeping patches to sustain more coseismic slip and higher slip rates than in the models with stronger rate-strengthening properties. Using rate-neutral properties for the creeping patches (supplemental figure S2) allows rupture to propagate through or around creeping patches with radii up to 10 km, rather than 8 km, but the 12 km radius case still stops rupture before it reaches the other end of the fault.

Figure 3.

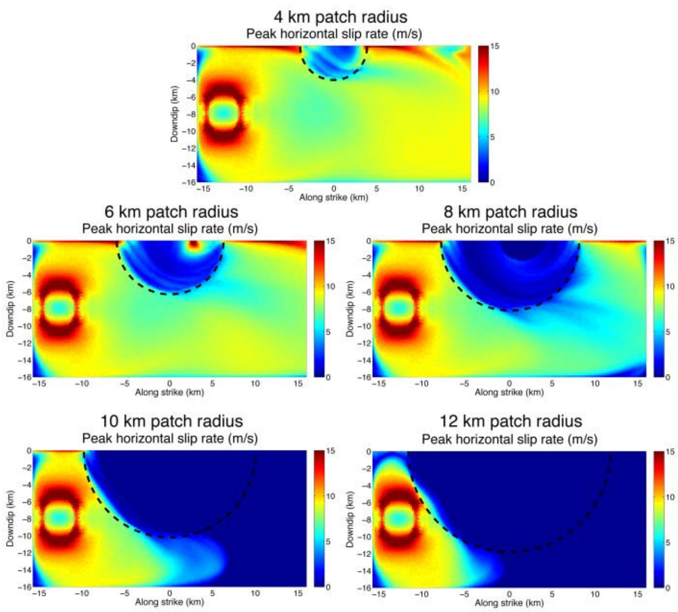

Figure 3. Plots of maximum horizontal slip rate for models of a rate-strengthening/creeping patch within an otherwise rate-weakening/locked fault. The dashed black line marks the edge of the creeping patch. The ring of high slip rate to the left of the fault represents the forced nucleation zone. Dynamic rupture progresses through the creeping patch in the 4 km radius model, whereas it wraps around the creeping patch and then propagates bilaterally inward in the 6 and 8 km radius models. The zone of high slip rate within the creeping patch in the 6 km radius model represents the coalescence of the rupture fronts propagating inward from either side. If the creeping patch is greater than 8 km in radius, it prevents the rupture from propagating to the other end of the fault.

Next we investigate the maximum slip rate for the set of models in which we extend the length of the fault by the same amount as we increase the radius of the creeping patch, thereby ensuring that the rupture front is able to build up the same amount of directivity before reaching the edge of the creeping patch, regardless of the patch radius. We show these results in in Figure 4. This additional energy due to directivity did not affect the ability of rupture to propagate across the entire fault. Creeping patch radii of greater than half the seismogenic thickness of the fault still arrested rupture propagation. The primary effect of extending the length of the fault was increased extent and amount of coseismic slip within the creeping patches.

Figure 4.

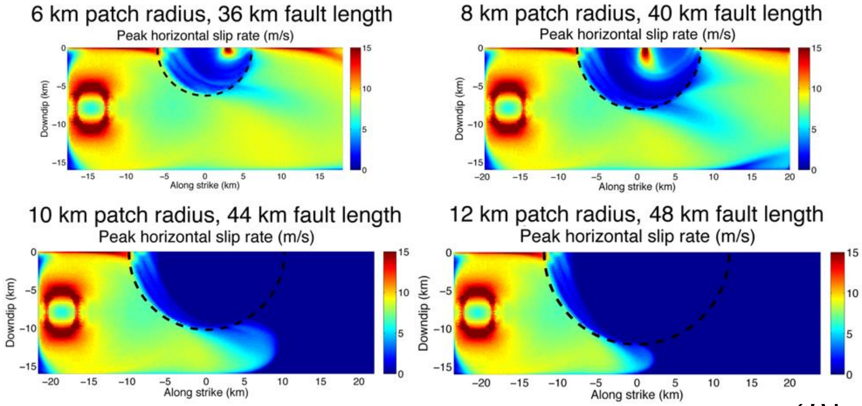

Figure 4. Plots of maximum horizontal slip rate for models of a rate-strengthening/ creeping patch within an otherwise rate-weakening/ locked fault, with the length of the fault scaled by the radius of the creeping patch. The ring of high slip rate to the left of the fault represents the forced nucleation zone. The dashed black line marks the edge of the creeping patch. Increasing the length of the fault has no first-order effect on rupture's ability to propagate along strike (compare to Figure 3), but the larger directivity effect that results from rupture propagating a larger distance before reaching the creeping patch allows for more coseismic slip within the creeping patch. The areas of particularly high slip rate within the creeping patch in the 6 and 8 km radius models represent the coalescence of two rupture fronts propagating inward from either side of the patch.

The models in which we increased the depth of the fault as we increased the radius of the creeping patch are shown in Figure 5. Keeping the distance between the base of the creeping patch and the base of the fault fixed allowed rupture to propagate through the full strike of the fault in all cases. However, rupture was unable to propagate all the way to the surface of the fault in the models with the largest patch radii. Increasing the basal depth of the fault also has little effect on the ability of the creeping patch to sustain coseismic slip.

Figure 5.

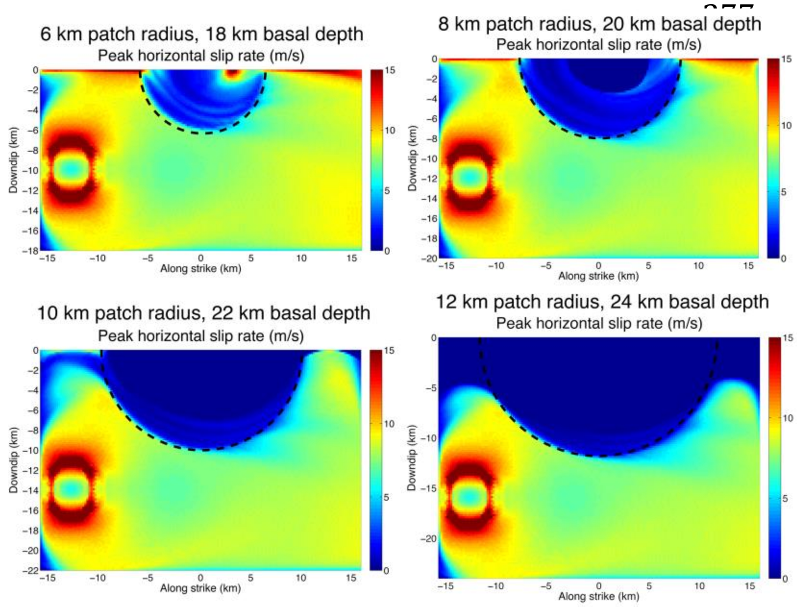

Figure 5. Plots of maximum horizontal slip rate for models of a rate-strengthening/creeping patch within an otherwise rate-weakening/locked fault, with the basal depth of the fault scaled by the radius of the creeping patch. The dashed black line marks the edge of the creeping patch. The ring of high slip rate to the left of the fault represents the forced nucleation zone. In all cases, rupture propagates along the full extent of the fault strike, but larger creeping patches prevent surface rupture. As in the set of models with a constant 16 km basal depth, smaller creeping patches sustain higher slip rates.

3.2 Locked Patch Within a Creeping Fault

The radius of a locked patch within a predominantly creeping fault has very little effect on the overall rupture behavior other than to increase the size of the slipping region. In all of these models (see Figure 6), rupture propagated to the edges of the locked patch, then died out within 1 km of the interface between the locked patch and the creeping zone. Even in the model with a 4 km locked patch radius, in which the radius of the forced nucleation zone was larger than the radius of the locked patch and dynamic rupture was forced into the rate-strengthening zone, rupture still stopped within 1 km of the edge of the forced nucleation zone. Implementing a weaker rate-strengthening effect (supplementary figure S3) for the creeping parts of the fault slightly increased how far coseismic slip was able to propagate into the creeping zone before coming to a halt, but this effect was not significant enough to allow full dynamic rupture through a rate-strengthening zone. For the most part, implementing rate-neutral friction in the creeping zones (supplementary figure S4) follows this pattern, with slightly more slip slightly further outside the locked patch. However, the 12 km radius case does have full rupture of the fault, since the area of creeping fault between the top of the locked patch and the free surface is small enough that waves from the rupture in the locked patch re able to interact with the free surface, producing high slip rates there (e.g. *Kaneko and Lapusta* [2010], *Hu et al*. [2019]) . Despite this effect at the surface, slip rates remain low between the top of the fault and the free surface.

Figure 6.

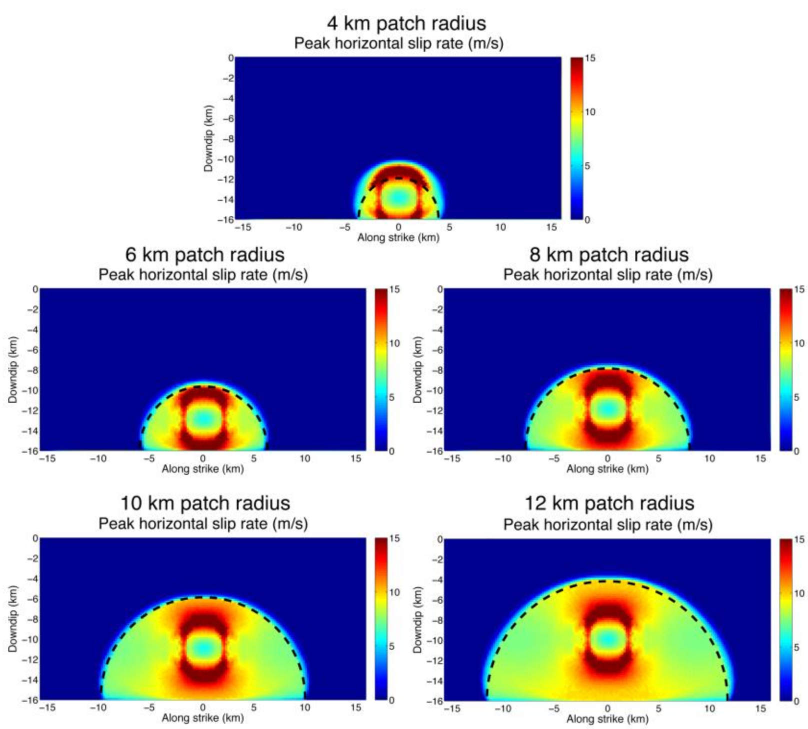

Figure 6. Plots of maximum horizontal slip rate for models of a locked/rate-weakening patch within an otherwise creeping/rate-strengthening fault. The dashed black line indicates the edge of the locked patch. The ring of highest slip rate in the center of the locked patch represents the forced nucleation zone. Note that regardless of the size of the locked patch, rupture does not propagate more than 1 km beyond the edge of the patch into the creeping zone – which is consistent with past work on high-strength asperities in low-stress faults (e.g. *Day* [1982]). In addition, in the 4 km patch radius model, the size of the forced nucleation zone is larger than the size of the locked patch, but even forced propagation into the creeping part of the fault does not result in self-sustaining rupture outside of the forced nucleation zone.

4 Discussion

We find that the dimensions of the creeping parts of a fault relative to the locked parts have a strong effect on the overall rupture behavior and extent. In particular, our results suggest there must be a critical width of locked fault through which full dynamic rupture can propagate around a creeping zone. If the narrowest dimension of the locked zone is between the base of the fault and the furthest down-dip edge of the creeping patch, as in the 10 and 12 km radius cases in Figure 3, along-strike rupture may be halted. Similarly, if the narrowest dimension is between the end of the fault and the nearest along-strike edge of the creeping patch, as in the 12 km radius case in Figure 5, rupture may be prevented from reaching the surface of the fault. This is very similar to studies of dynamic rupture propagating around high-stress or geometrical asperities in locked strike-slip faults (e.g. *Day* [1982], *Das and Kostrov* [1983]); this presents the possibility of treating creeping patches as generalized barriers in hazard assessments.

That said, in the specific context of rate-strengthening creeping patches, this barrier effect is a result of how the energy budget of a rupture front is divided. A rupture propagating along a homogeneous rate-weakening fault builds up energy ahead of the rupture front in the direction of rupture, and can expend most of that energy on seismic radiation and increasing its propagation speed, rather than on fracture energy or friction. Creeping patches with smaller radii do not pose much of an interruption to directivity and to this buildup of energy, which is why fracturing and slipping into the rate-strengthening patch do not use so much of the energy budget such that none is left for propagation and radiation. However, a creeping patch with a large radius alters the energy balance both by requiring more energy to go into fracturing through the creeping area, and by decreasing the area of fault that is building up more energy ahead of the rupture front. Thus, the rupture becomes less energetic overall, and is spending more of the remaining energy on fracture and less on propagation and radiation, which ultimately leads to the rupture dying out in the narrow locked zone and not propagating as far into the creeping patch.

We illustrate this effect in Figure 7. There is not currently a rate-state friction-specific equation for energy budget, but *Ryan and Oglesby* [2014] show that, at coseismic rupture speeds, rate-state friction and slip-weakening friction behave nearly identically. Therefore, we adapt our data to the slip-weakening friction formulation of *Kanamori and Rivera* [2006]. The total energy available for rupture propagation is given as $E_{to} = ½(\tau_1\text{-}\tau_2)DA$, where τ_1 is initial shear stress, τ_2 is final shear stress, D is fault displacement, and A is fault area. The fracture energy in the rupture front is given as $E_g = (\tau_p - \tau_1)D_CA/2$. where τ_p is the yield stress, τ_1 is the initial shear stress, D_C is the critical slip-weakening distance, and A is the fault area. In adapting these theoretical formulas to plot model results, we use the slip-weakening friction distances and coefficients from *Ryan and Oglesby* [2014] that correspond to the rate-state parameters in this study. We set τ_0 to be the initial pre-rupture shear stress at each node on the fault, τ_1 as the yield stress at each node, and τ_2 as the final shear stress at each node after the fault has fully weakened. D is the total displacement at each fault node; if D is larger than the critical weakening parameter Dc, we set D = Dc. Since we calculate these parameters at each fault node, we use the area of one on-fault element for the parameter A.

These formulas represent the energy budget of an entire fault for an entire earthquake, so it is not rigorously correct to use them to indicate the energy budget for individual time-steps at many finite points on the fault. However, they still provide a general qualitative insight into the relative partitioning of energy during fault rupture, given that we are trying to illustrate a first-order effect. Figure 7 clearly shows that the total available rupture energy (E_{to}) drops significantly as the rupture front reaches the creeping patch, while fracture energy (E_g) rises, as does the ratio of E_g to E_{to}.

Figure 7.

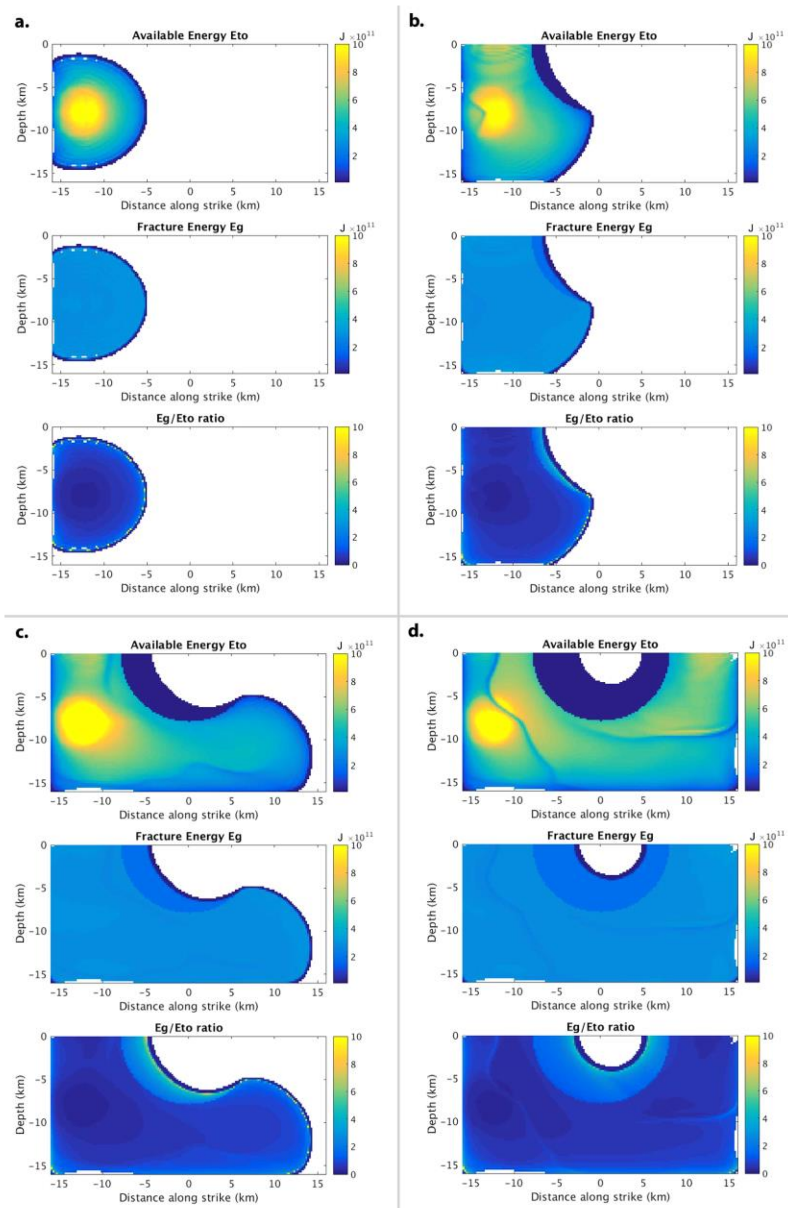

Figure 7. Snapshots of a rough estimate of the energy budget as rupture progresses, for the 8 km creep radius case. E_{to} is the available energy for rupture, and E_g is the fracture energy in the rupture front, based on equations from *Kanamori and Rivera* [2006]. We plot energy budget in parts of the fault which are slipping at faster than 1 mm/s. The rupture front itself is most clearly visible in the Eg/Eto ratio plots, where there is a sharp contrast between dark blue and yellow/orange.

a. The rupture so far has been entirely in the locked zone. E_g and E_{to} are comparable.

b. The rupture front encounters the creeping patch. Both E_{to} and E_g drop, but E_g is now higher than E_{to}. The ratio goes up.

c. Rupture progresses faster through the locked zone than the creeping patch. E_{to} and E_g are still comparable in the rate-weakening zones. Both are still lower in the creeping patch, but the E_g/E_{to} ratio remains high.

d. The locked zones of the fault have completely ruptured, and slow rupture continues into the unfavorable creeping patch. The total energy remains low, but the E_g/E_{to} ratio remains high.

As a test of this energy budget imbalance and critical width effect, we conducted a model in which a creeping patch with a 12 km radius is embedded in a fault that is as long as the 12 km radius case in Figure 3 and as deep as the 12 km radius case in Figure 5, thus eliminating any major narrowing of the locked zone. In this model, the results of which are shown in Figure 8, rupture propagated from end to end of the fault, and from base to surface. Because it propagated through a much larger locked area than in the other models, this rupture front was able to build up enough energy that it was able to propagate much further into the creeping patch than in any of our other models.

Figure 8.

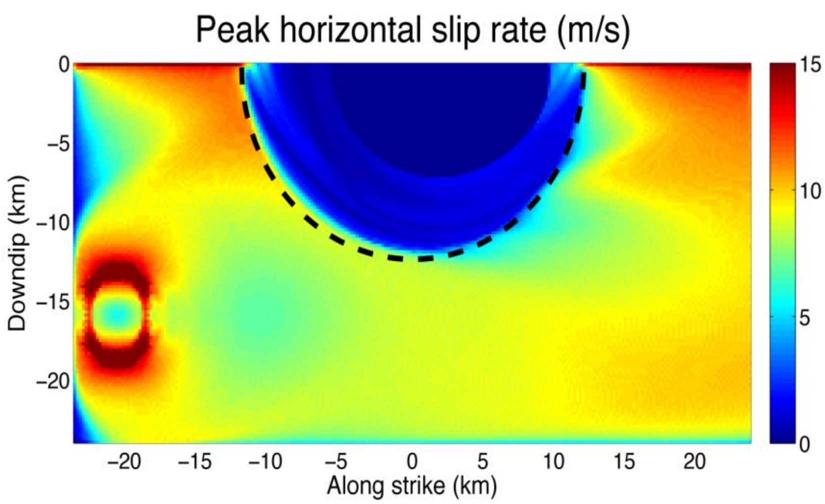

Figure 8. Maximum horizontal slip rate for a model with a creeping patch with a 12 km radius embedded in an otherwise locked fault, with both the fault length and basal depth scaled up to accommodate the large patch radius. The edge of the creeping patch is indicated by the dashed black line. A 12 km patch radius arrested along-strike rupture in Figure 3, and up-dip rupture in Figure 5, but in this model, rupture is able to reach both the surface and the far end of the fault.

The balance of the energy budget is also why the cases in which the rate-weakening part of the fault is completely surrounded by rate-strengthening all result in rupture stopping within a short distance of the edge of the locked patch. In these cases, the available energy for rupture still decreases when rupture reaches the rate-strengthening zone, but here, the rate-strengthening zone is most of the fault. While the fracture energy initially does rise relative to the rupture energy, the lack of ongoing rupture in a rate-weakening zone elsewhere on the fault, and therefore the lack of energy accumulation ahead of the rupture front, decreases the total energy in the system, and the rupture front is not able to sustain the level of fracture energy necessary to break into the creeping patch. In these cases, rupture halts far more quickly when it reaches the creeping zone than it does in the cases with a creeping patch surrounded by a locked fault.

5 Conclusions

We find that the presence of a creeping patch within a locked fault, and vice versa, can have a controlling effect on the ability of rupture to propagate through the entire fault. In particular, the down-dip width between the bottom of the creeping zone and the base of the fault is the controlling factor. If the locked zone at depth is too narrow, then the overall energy budget of the rupture decreases, and more of the remaining energy is spent on fracture as opposed to propagation and radiation, which can lead to arrest of the rupture front. In the case of a locked patch within a creeping fault, this reduction and re-balancing of the energy budget is almost instantaneous when rupture reaches the edge of the locked patch, which results in near immediate cessation of rupture propagation. We also find that some coseismic slip through a creeping zone is possible in cases where the rupture front is not forced to narrow much around the creeping zone, though the amount of slip is less than in locked areas, and the associated slip rate is slower (except in the small area where inward-propagating rupture fronts meet, as shown in figures 3, 4, and 5).

Although our models are extremely simple when compared to a real-world fault, and although they do not account for the difference in interseismic stress and strain accumulation on a creeping zone as opposed to a locked one (which would further reduce the ability of rupture to propagate into the creeping zones, e.g. *Lozos and Funning* [submitted to this issue]), they still provide indications as to possible rupture extents. In a case where the locked patches are surrounded entirely by creep, dynamic rupture is likely to be confined to those locked patches, which means an end-to-end dynamic rupture of the entire fault is unlikely, and that observed surface displacement is more likely to be postseismic than coseismic. Our case-specific simulations of Hayward Fault ruptures show these same behaviors even within a more complex model setup [*Lozos and Funning*, submitted to this issue]. However, if the creeping patches of a given fault are small and surrounded by locked zones, they may be able to sustain coseismic slip, and possibly even produce a pulse of seismic radiation. Our models highlight the importance of knowing the geometry of the creeping and locked parts of a partially-creeping fault in assessing potential rupture lengths and amounts of coseismic surface displacement. We emphasize that any dynamic rupture models on specific real-world partially-creeping faults should incorporate this complexity with as much detail as possible.

Acknowledgments, Samples, and Data

We would like to thank Kenny Ryan and Michael Barall for their invaluable assistance in setting up these simulations. We also thank Jim Dieterich, Ruth Harris, and Norm Abrahamson for insightful conversations and comments on this work.

We did not directly use any external datasets, nor did we collect or generate new data in this modeling study.

References

Barall, M. (2009). A grid-doubling technique for calculating dynamic three-dimensional spontaneous rupture on an earthquake fault, *Geophysical Journal International* **178**, 845–859. doi: 10.1111/j.1365-246X.2009.04190.x

Barbot, S., Fialko, Y., & Bock, Y. (2009). Postseismic deformation due to the Mw 6.0 2004 Parkfield earthquake: Stress-driven creep on a fault with spatially variable rate-and-state friction parameters. *Journal of Geophysical Research: Solid Earth*, *114*(B7). doi: 10.1029/2008JB005748

Barnhart, W. D., Hayes, G. P., and Gold, R. D. (2019), The July 2019 Ridgecrest, California, Earthquake Sequence: Kinematics of Slip and Stressing in Cross-Fault Ruptures. Geophys. Res. Let., *46*(21), 11859-11867. doi: 10.1029/2019GL084741

Bilham, R., and B. Castillo (2020). The July 2019 Ridgecrest, California, Earthquake Sequence Recorded by Creepmeters: Negligible Epicentral Afterslip and Prolonged Triggered Slip at Teleseismic Distances. Seism. Res. Let., doi:10.1785/0220190293.

Das, S., & Kostrov, B. V. (1983). Breaking of a single asperity: rupture process and seismic radiation. *Journal of Geophysical Research: Solid Earth*, *88*(B5), 4277-4288. doi: 10.1029/JB088iB05p04277

Day, S. M. (1982). Three-dimensional simulation of spontaneous rupture: the effect of nonuniform prestress. *Bulletin of the Seismological Society of America*, *72*(6A), 1881-1902.

Dieterich, J. H. (1978). Time-dependent friction and the mechanics of stick-slip, *Pure and Applied Geophysics* **116**, 790-806.

Floyd, M. A., Walters, R. J., Elliott, J. R., Funning, G. J., Svarc, J. L., Murray, J. R., ... & Johanson, I. A. (2016). Spatial variations in fault friction related to lithology from rupture and afterslip of the 2014 South Napa, California, earthquake. *Geophysical Research Letters*, *43*(13), 6808-6816. doi: 10.1002/2016GL069428

Funning, G. J., R. Bürgmann, A. Ferretti and F. Novali (2009), Mapping the extent of fault creep along the Hayward-Rodgers Creek-Maacama fault system using PS-InSAR, Eos Trans. AGU, 90(52), Fall Meet. Suppl., Abstract G34A-08.

Harris, R. A., & Segall, P. (1987). Detection of a locked zone at depth on the Parkfield, California, segment of the San Andreas fault. *Journal of Geophysical Research: Solid Earth*, *92*(B8), 7945-7962.

Harris, R. A., and S. M. Day (1993). Dynamics of fault interaction: parallel strike-slip faults, *Journal of Geophysical Research* **98,** 4461-4472.

Harris, R. A., Barall, M., Archuleta, R., Dunham, E., Aagaard, B., Ampuero, J. P., ... & Day, S. (2009). The SCEC/USGS dynamic earthquake rupture code verification exercise. *Seismological Research Letters*, *80*(1), 119-126.

Harris, R. A., Barall, M., Aagaard, B., Ma, S., Roten, D., Olsen, K., ... & Ampuero, J. P. (2018). A suite of exercises for verifying dynamic earthquake rupture codes. *Seismological Research Letters*, *89*(3), 1146-1162.

Harris, R., Barall, M., Ponce, D. A., Moore, D. E., Graymer, R. W., Lockner, D. A., Morrow, C. A., and Funning, G. (2019). Dynamic Rupture Scenarios of Large Earthquakes on the Hayward Fault System, California, using Observations from Geology and Geodesy. *AGUFM*, *2019*, S33A-08.

Hu, F., Oglesby, D. D., & Chen, X. (2019). The sustainability of free-surface-induced supershear rupture on strike-slip faults. *Geophysical Research Letters*, *46*(16), 9537-9543.

Kame, N., J. R. Rice, and R. Dmowska (2003). Effects of pre-stress state and rupture velocity on dynamic fault branching, *Journal of Geophysical Research* **108,** 2265, doi: 10.1029/2002JB002189.

Kanamori, H., & Rivera, L. (2006). Energy partitioning during an earthquake. doi: 10.1029/170GM03

Kaneko, Y., Lapusta, N., & Ampuero, J. P. (2008). Spectral element modeling of spontaneous earthquake rupture on rate and state faults: Effect of velocity-strengthening friction at shallow depths. *Journal of Geophysical Research: Solid Earth*, *113*(B9). doi: 10.1029/2007JB005553

Kaneko, Y., & Lapusta, N. (2010). Supershear transition due to a free surface in 3-D simulations of spontaneous dynamic rupture on vertical strike-slip faults. *Tectonophysics*, *493*(3-4), 272-284. doi: 10.1016/j.tecto.2010.06.015

Kaneko, Y., Fialko, Y., Sandwell, D. T., Tong, X., & Furuya, M. (2013). Interseismic deformation and creep along the central section of the North Anatolian fault (Turkey): InSAR observations and implications for rate-and-state friction properties. *Journal of Geophysical Research: Solid Earth*, *118*(1), 316-331. doi: 10.1029/2012JB009661

Kodaira, S., No, T., Nakamura, Y., Fujiwara, T., Kaiho, Y., Miura, S., ... & Taira, A. (2012). Coseismic fault rupture at the trench axis during the 2011 Tohoku-oki earthquake. *Nature Geoscience*, *5*(9), 646-650. doi: 10.1038/ngeo1547

Lienkaemper, J. J., Borchardt, G., & Lisowski, M. (1991). Historic creep rate and potential for seismic slip along the Hayward fault, California. *Journal of Geophysical Research: Solid Earth*, *96*(B11), 18261-18283. doi: 10.1029/91JB01589

Lienkaemper, J. J., McFarland, F. S., Simpson, R. W., & Caskey, S. J. (2014). Using surface creep rate to infer fraction locked for sections of the San Andreas fault system in northern California from alignment array and GPS data. *Bulletin of the Seismological Society of America*, *104*(6), 3094-3114. doi: 10.1785/0120140117

Lienkaemper, J. J., DeLong, S. B., Domrose, C. J., & Rosa, C. M. (2016). Afterslip behavior following the 2014 M 6.0 South Napa earthquake with implications for afterslip forecasting on other seismogenic faults. *Seismological Research Letters*, *87*(3), 609-619. doi: 10.1785/0220150262

Lozos, J. C., D. D. Oglesby, B. Duan, and S. G. Wesnousky (2011). The effects of fault bends on rupture propagation: a geometrical parameter study, *Bulletin of the Seismological Society of America* **101***,* 385-398. doi: 10.1785/0120100029

Lozos, J. C., Dieterich, J. H., & Oglesby, D. D. (2014). The effects of d_0 on rupture propagation on fault stepovers. *Bulletin of the Seismological Society of America*, *104*(4), 1947-1953. doi: 10.1785/0120130305

Lozos, J. C., Harris, R. A., Murray, J. R., & Lienkaemper, J. J. (2015). Dynamic rupture models of earthquakes on the Bartlett Springs Fault, Northern California. *Geophysical Research Letters*, *42*(11), 4343-4349. doi: 10.1002/2015GL063802

Lozos, J. C., and G. J. Funning (submitted). Dynamic rupture modeling on the Hayward Fault, northern California – estimating coseismic and postseismic hazards of partially creeping faults, submitted to Journal of Geophysical Research.

McCaffrey, R., Wallace, L. M., & Beavan, J. (2008). Slow slip and frictional transition at low temperature at the Hikurangi subduction zone. *Nature Geoscience*, *1*(5), 316-320. doi: 0.1038/ngeo178

Moore, D. E., & Rymer, M. J. (2007). Talc-bearing serpentinite and the creeping section of the San Andreas fault. *Nature*, *448*(7155), 795-797. doi: 10.1038/nature06064

Moore, D. E., McLaughlin, R. J., & Lienkaemper, J. J. (2018). Serpentinite-Rich Gouge in a Creeping Segment of the Bartlett Springs Fault, Northern California: Comparison With SAFOD and Implications for Seismic Hazard. *Tectonics*, *37*(12), 4515-4534. doi: 10.1029/2018TC005307

Murray, J. R., Minson, S. E., & Svarc, J. L. (2014). Slip rates and spatially variable creep on faults of the northern San Andreas system inferred through Bayesian inversion of Global

Positioning System data. *Journal of Geophysical Research: Solid Earth*, *119*(7), 6023-6047. doi: 10.1002/2014JB010966

Nielsen, S. B., Carlson, J. M., & Olsen, K. B. (2000). Influence of friction and fault geometry on earthquake rupture. *Journal of Geophysical Research: Solid Earth*, *105*(B3), 6069-6088. doi: 10.1029/1999JB900350

Noda, H., and N. Lapusta (2013). Stable creeping fault segments can become destructive as a result of dynamic weakening, *Nature* **493**, 518-521. doi: 10.1038/nature11703

Oglesby, D. (2008). Rupture termination and jump on parallel offset faults. *Bulletin of the Seismological Society of America*, *98*(1), 440-447. doi: 10.1785/0120070163

Ross, Z.E., Idini, B., Jia, Z., Stephenson, O.L., Zhong, M., Wang, X., Zhan, Z., Simons, M., Fielding, E.J., Yun, S.H. and Hauksson, E. (2019). Hierarchical interlocked orthogonal faulting in the 2019 Ridgecrest earthquake sequence. Science, *366*(6463), pp.346-351. doi: 10.1126/science.aaz0109

Ruina, A. (1983). Slip instability and state variable friction laws*, Journal of Geophysical Research* **88**, 10359-10370. doi: 10.1029/JB088iB12p10359

Ryan, K. J., & Oglesby, D. D. (2014). Dynamically modeling fault step overs using various friction laws. *Journal of Geophysical Research: Solid Earth*, *119*(7), 5814-5829. doi: 10.1002/2014JB011151

Schulz, S. S., Mavko, G. M., Burford, R. O., & Stuart, W. D. (1982). Long-term fault creep observations in central California. *Journal of Geophysical Research: Solid Earth*, *87*(B8), 6977-6982. doi: 10.1029/JB087iB08p06977

Schmidt, D. A., R. Bürgmann, R. M. Nadeau and M. d'Alessio (2005), Distribution of aseismic slip rate on the Hayward fault inferred from seismic and geodetic data, *J. Geophys. Res.*, 110, B08406, doi: 10.1029/2004JB003397

Shibazaki, B., & Shimamoto, T. (2007). Modelling of short-interval silent slip events in deeper subduction interfaces considering the frictional properties at the unstable—Stable transition regime. *Geophysical Journal International*, *171*(1), 191-205. doi: 10.1111/j.1365-246X.2007.03434.x

Stephenson, O., & Lapusta, N. (2018). Exploring the Possibility of Dynamic Rupture Through the Creeping Section of the San Andreas Fault in a Simplified 2D Model. *AGUFM*, *2018*, T43B-06.

Waldhauser, F., Ellsworth, W. L., Schaff, D. P., & Cole, A. (2004). Streaks, multiplets, and holes: High-resolution spatio-temporal behavior of Parkfield seismicity. *Geophysical Research Letters*, *31*(18). doi: 10.1029/2004GL020649

Wang, H., Liu, M., Duan, B., & Cao, J. (2020). Rupture Propagation along Stepovers of Strike-Slip Faults: Effects of Initial Stress and Fault Geometry. *Bulletin of the Seismological Society of America*, *110*(3), 1011-1024. doi: 10.1785/0120190233

Wei, S., Barbot, S., Graves, R., Lienkaemper, J. J., Wang, T., Hudnut, K., ... & Helmberger, D. (2015). The 2014 Mw 6.1 South Napa earthquake: A unilateral rupture with shallow asperity and rapid afterslip. *Seismological Research Letters*, *86*(2A), 344-354. doi: 10.1785/0220140249